RSC Advances

ROYAL SOCIETY OF CHEMISTRY

www.rsc.org/advances

Layer-by-layer assembled protein nanotube shows extremely high adsorption capacity for DNA molecules.
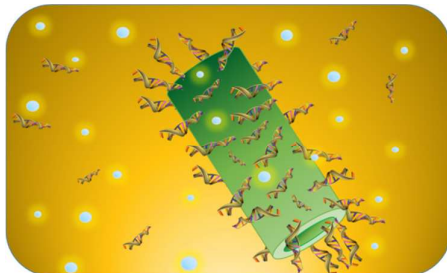
ARTICLE TYPE

Layer-by-layer assembled protein nanotubes with high DNA affinity

Peipei Jiao[a], Yanli Guo[*a], Aihua Niu[a], Xiaofeng Kang[*a]

5 **ABSTRACT**

In this research, protein nanotube with high affinity for DNA molecules was prepared by alternate layer-by-layer (LbL) assembly of human serum albumin (HSA) and polyethylenimine (PEI). The well-defined hollow cylinder $(PEI/HSA)_5PEI$ nanotubes with outer diameter 455 ± 13 nm, inner diameter 275 ± 35 nm, wall thickness 151 ± 7 nm and length 5.6 ± 0.9 μm were characterized by Scanning electron microscope
10 (SEM), Transmission electron microscope (TEM), Fourier transform infrared spectroscopy (FT-IR) and Energy dispersive spectroscopy (EDS). Under optimal condition, the maximum adsorption capacity of protein nanotube for $polyA_{25}$ was 606.0 mg/g, which was far higher than the reported nanoparticles. The rates of adsorption were found to conform to the pseudo-second-order kinetics and intra-particle diffusion models with good correlation. The equilibrium adsorption data fitted well with Langmuir isotherm model.
15 The DNA release from $DNA/(PEI/HSA)_5PEI$ nanotubes was associated with the ionic strength and pH in the solution.

1. Introduction

The adsorption or immobilization nucleic acid on solid surfaces is essential in a wide range of researches including DNA chip
20 technology, DNA hybridization and gene delivery[1-6]. The inherent merits of nanotube, for example, unique hollow structure, distinct inner and outer surfaces as well as two open-end terminals, make it to be a promising nanomaterial for bimolecular immobilization and delivery[7]. Inorganic nanotubes
25 such as carbon nanotubes[8], silica nanotubes[9] and magnetic nanotubes[10] have been developed for gene vectors. But their biomedical applications are limited due to the lack of biocompatibility and biodegradability. It could be a good trategy to synthesize biological nanotubes. Some biological nanotubes
30 such as lipid nanotubes[11] have been reported for this propose. However, protein nanotubes with DNA affinity are largely unexplored, thus is addressed in this paper.

Currently, a popular approach to prepare protein nanotubes is the combination of layer-by-layer (LbL) assembly technique with
35 template method. Exploiting the electrostatic attraction, oppositely charged polyelectrolytes and biomacromolecules can build up multilayer into the pores of nanoporous membrane, such as anodic aluminium oxide (AAO) or track-etch polycarbonate (PC). The hollow protein nanotubes are obtained by subsequently
40 removing the template[12-14]. This technique provides a simple and versatile means that can tune the thin films precisely on nanometer scales, and the synthesized tubular structures own tailored shapes and sizes.

Protein nanotubes were functionalized by assembling different
45 molecules on the internal wall to realize target molecules capturing. For example, nanotubes assembled by human serum albumin (HSA) and poly-L-arginine (PLA) could bind the zinc (II) protoporphyrin IX to the HSA component in the cylindrical wall[15]. The hybrid HSA/PLA nanotubes bearing single avidin
50 layer as an internal wall captured biotin-labelled nanoparticles into the central channel[15]. The nanotubes with an antibody surface interior entrapped human hepatitis B virus with size selectivity[16].

One of the methods of DNA immobilization has been reported
55 based on ionic interaction occurring between the negatively charged groups present on the DNA and positive charges covering the surface[17]. Polyethylenimine (PEI) is a kind of cationic polyelectrolyte and the branched structure of PEI contains nitrogen at every third atom, resulting in a high charge
60 density. PEI is often considered as the most prominent polymer capable of gene transfection[18] and DNA immobilization[19]. Therefore, we can expect that protein/PEI hybridized nanotubes with PEI on the inner and outer surfaces will provide the high efficient DNA loading.
65 In this article, protein nanotubes $((PEI/HSA)_5PEI)$ were prepared and the adsorption and release performances for oligonucleotides were investigated. Kinetic and isotherm models were applied to the experimental data for a better understanding of the binding process.

70 ## 2. Experimental

2.1. Chemicals and materials

Polyethylenimine (PEI, Mw = 750,000, 50% (w/v) in water), human serum albumin (HSA, 96%-99%) and calf thymus DNA (ctDNA) were purchased from Sigma-Aldrich. The track-etch
75 nanoporous PC membrane (No. 28420636, circle membrane

diameter 25 mm, pore diameter 400 nm) was purchased from DNA-SYN Biotechnology Synthesis Lab (Beijing, China). The water was deionised (18.2 MΩ cm⁻¹) using purification Milli-Q system (Millipore, USA). All chemicals were used as received without further purification. Experiments were all carried out at 25 ± 2 ºC.

2.2. Preparation of protein nanotubes

(PEI/HSA)₅PEI nanotubes were fabricated in PC nanopores by the revised LbL assembly according to previous method[15]. Briefly, PC membrane was placed into a filter. 10 mL 1 mg/mL PEI was firstly flowed through at the speed of 0.25 mL/min using a syringe pump. Then the loosely adsorbed PEI was washed by 10 mL pH 7.4 PB at the rate of 1 mL/min. Following this, the membrane was dried under a stream of N₂. In next step, 2 mg/mL HSA dissolved in pH 7.4 PB solution was injected (10 mL, 0.5 mL/min) through the membrane with assembled PEI layer. After injection of pH 7.4 PB solution (10 mL, 1 mL/min) to remove the loosely bound HSA, the membrane was again N₂ dried. Between each deposition steps, a cotton swab with water was used to eliminate the adsorption of PEI and HSA on the top and bottom of PC surfaces. After repeating 5.5-cycle injection, the membrane was dried in vacuum for 12 h (0.09 Mpa) and immersed in DMF subsequently. The PC was quickly dissolved and the (PEI/HSA)₅PEI nanotubes were precipitated. The liberated nanotubes were washed 3-5 times with DMF and the supernatants were discarded. Finally, the lyophilized (PEI/HSA)₅PEI nanotubes powder was yielded by freeze-dried the dispersion under vacuum (-60 ºC, < 20 Pa).

2.3. Characterization of protein nanotubes

For TEM observation, the dispersion of (PEI/HSA)₅PEI stained with 3% phosphotungstic acid was observed on a H600 electron microscope (Hitachi, Japan) at 75 kV. The SEM and EDS images were obtained using a JSM-6390 electron microscope (JEOL, Japan) by analyzing the lyophilized sample that sputter-coated with gold using an ion sputter (E1010, Hitachi). FT-IR spectra were recorded by using a TENSOR 27 FT-IR spectrophotometer (Bruker, German). UV-vis spectroscopy measurements were conducted using infinite M200 PRO (TECAN, Switzerland) to evaluate the adsorption and desorption experiments.

2.4. Adsorption experiments

The adsorption property of (PEI/HSA)₅PEI for DNA was studied. PolyA₂₅ was selected as typical DNA. A stock solution of 1 mg/mL was prepared and diluted to the required concentrations at pH 7.4. In each experiment, 200 μL polyA₂₅ solution was added into a 1.5 mL centrifuge tube with 0.1 mg (PEI/HSA)₅PEI nanotubes. The mixtures were stirred continuously using an orbital shaker. At regular intervals, polyA₂₅ concentration in supernatant was determined by infinite M200 PRO at 260 nm after centrifugation with 6000 rpm. The amount of polyA₂₅ adsorbed onto (PEI/HSA)₅PEI nanotubes denoted as q_e (mg/g) was calculated using the following:

$$q_e = \frac{(C_0 - C_t)V}{m} \qquad (1)$$

Where C_o and C_t is the initial and equilibrium concentration of polyA₂₅ (mg/L), respectively, V (L) is the volume of polyA₂₅ solution and m (g) is the mass of (PEI/HSA)₅PEI nanotubes.

Effect of pH ranging from 4.7 to 11 was performed using 108 mg/L polyA₂₅. Adsorption isotherm was studied using polyA₂₅ solutions with concentrations ranging from 22 mg/L to 500 mg/L.

2.5. Release experiments

The DNA/(PEI/HSA)₅PEI nanotubes complexes were prepared by mixing 0.1 mg (PEI/HSA)₅PEI nanotubes with 200 μL 108 mg/L polyA₂₅ at pH 7.4 for 1 h. The complexes were collected with centrifugation of 6000 rpm and then dispersed in 200 μL of PB buffer solution at pH 7.4 and pH 5.7 in the presence of NaCl (0-1.5 M), respectively. At regular intervals, the desorbed polyA₂₅ in solution was determined by measuring the supernatant at 260 nm. The ratio of DNA release from complexes was calculated as:

$$\text{Release } (\%) = \frac{C_t V}{q_e m} \qquad (2)$$

Where C_t (mg/L) is the polyA₂₅ concentration in solution at t time, q_e (mg/g) is the pre-adsorbed amount of polyA₂₅ onto (PEI/HSA)₅PEI nanotubes, V (L) is the volume of the solution, m (g) is the mass of (PEI/HSA)₅PEI nanotubes.

The adsorption and release measurements were conducted in triplicate and reported as the mean values ± standard deviation (SD).

3. Results and discussion

3.1. Characterization of (PEI/HSA)₅PEI nanotubes and DNA/(PEI/HSA)₅PEI nanotubes complexes

SEM images of (PEI/HSA)₅PEI nanotubes (Fig. 1A) displayed the well-defined hollow cylinders with outer diameter of 455 ± 13 nm, inner diameter of 275 ± 35 nm and wall thickness of 151 ± 7 nm. The outer diameter was dependent on the PC template used, thus the nanotube size was controlled by the pore size. The (PEI/HSA)₅PEI nanotubes could be considered as the eleven-layered cylinder model, in which each HSA layer had a single-protein thickness. The HSA dimension was assumed to be 8 nm from the single crystal structure[20,21] and thus the thickness of PEI layer was calculated as 18.5 nm. This value was between the reported values for polyelectrolyte layers fabricated into porous template[15]. From the TEM image in Fig. 1B, a good tube structure was observed. The length was estimated to be 5.6 ± 0.9 μm, close to the PC template thickness (6 μm). Fig. 1C showed the FT-IR spectra of the fabricated nanotubes and HSA. In spectrum of HSA, peaks at 1660 cm⁻¹ and 1527 cm⁻¹ were the characteristic adsorptions of the C=O stretching vibration and the in-phase bending of N-H bond coupled with stretching of C-N bond in amide, respectively. The presence of peaks at 3400 cm⁻¹ and 2940-2830 cm⁻¹ was contributed to N-H stretching and C-H stretching vibrations[22]. Above results confirmed that the HSA layers were successfully assembled. Fig. 1D exhibited the EDS spectra of nanotubes. The main compositions of carbon, nitrogen, oxygen and sulfur were detected, indicating that the expected distributions of PEI and HSA existed.

The nanotubes with interior and exterior surfaces had cationic charges that could strongly bind the negatively charged DNA

through electrostatic interaction. Fig. 2 showed the TEM images
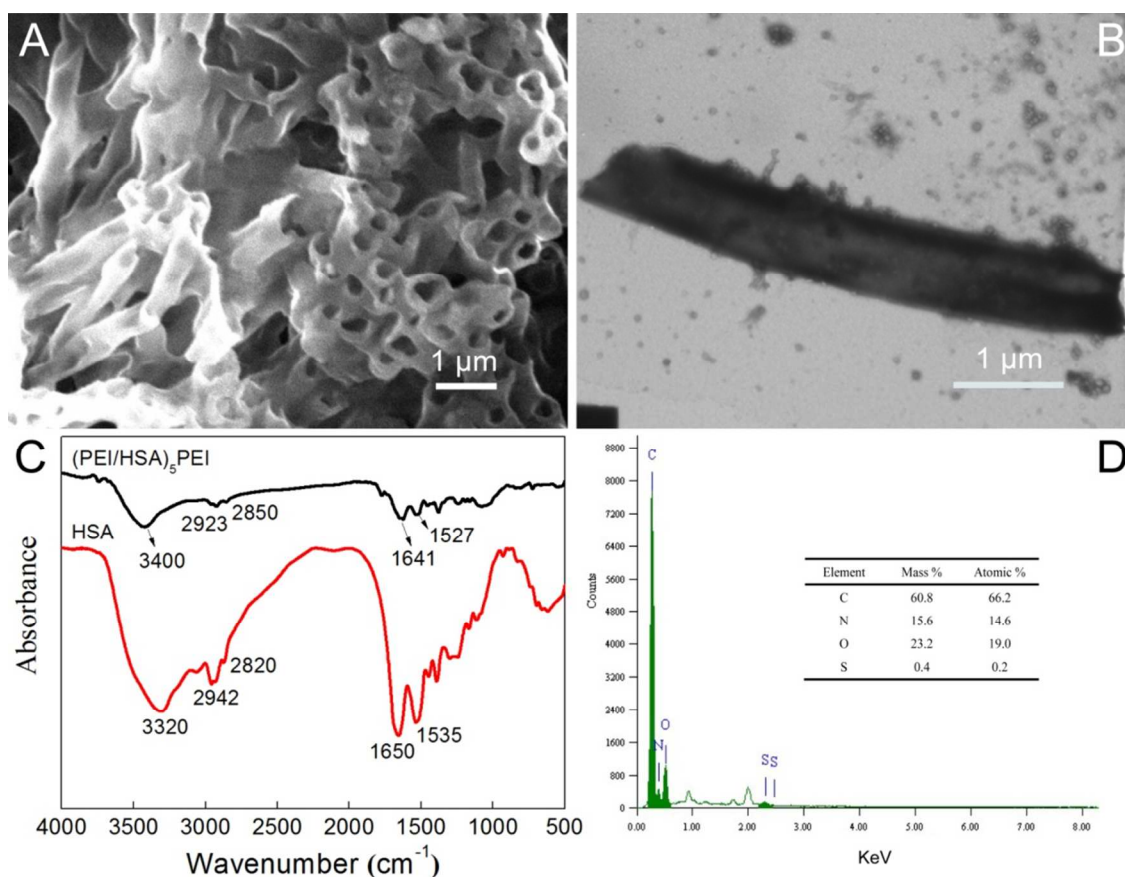
Fig. 1 (A) SEM and (B) TEM images of $(PEI/HSA)_5PEI$ nanotubes, (C) FT-IR spectra of $(PEI/HSA)_5PEI$ nanotubes and HSA, (D) EDS spectra of
5 $(PEI/HSA)_5PEI$ nanotubes, The inset is the elemental percentage.

of DNA/$(PEI/HSA)_5PEI$ nanotubes complexes. Compared with
$polyA_{25}$ (Fig. 2A), the detail structure was clearly demonstrated
by using the ctDNA. Indicated by black arrow in Fig. 2B, the
adsorbed ctDNA chains were visible.

10 **3.2. Effect of pH**

Since electrostatic interaction plays a key role in determining the
binding between DNA and nanotubes, it is necessary to study the
pH effect on the adsorption. From Fig. 3, it was found that
$polyA_{25}$ binding decreased slightly as the pH increased. For
15 example, the binding reduced from 94.8% to 87% by raising the
pH from 4.7 to 11. The $(PEI/HSA)_5PEI$ nanotubes surfaces are
terminated by primary, secondary and tertiary amino groups of
PEI and the pK_a values of these groups are around 9, 8 and 6–7,
correspondingly[23,24]. For $polyA_{25}$, it always maintains negative
20 charges in the pH tested for the phosphate group[25]. At pH below
9, amino groups were protonated to give a highly positively
charged surface. As pH above 10, deprotonation made the
decrease of adsorbed polyanion DNA.

3.3. Adsorption Kinetics

25 The time-dependent adsorption kinetics of the $(PEI/HSA)_5PEI$
nanotubes for $polyA_{25}$ was investigated. As shown in Fig. 4, the
amount of adsorbed $polyA_{25}$ increased rapidly in initial time, and
then increased gradually until reached the maximum. For lower
concentration of 22 mg/L, the time to reach the equilibrium was
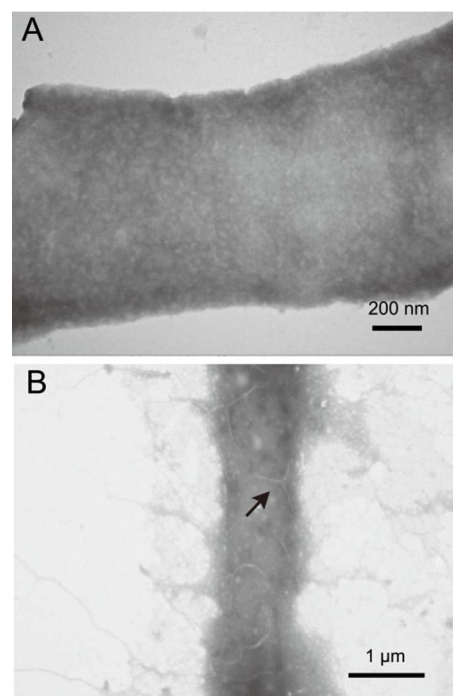
30 **Fig. 2** TEM images of $polyA_{25}$ (A) and ctDNA (B) complex with
$(PEI/HSA)_5PEI$ nanotubes in pH7.4 PB solution. Black arrow indicates
the adsorbed ctDNA chains onto nanotube.
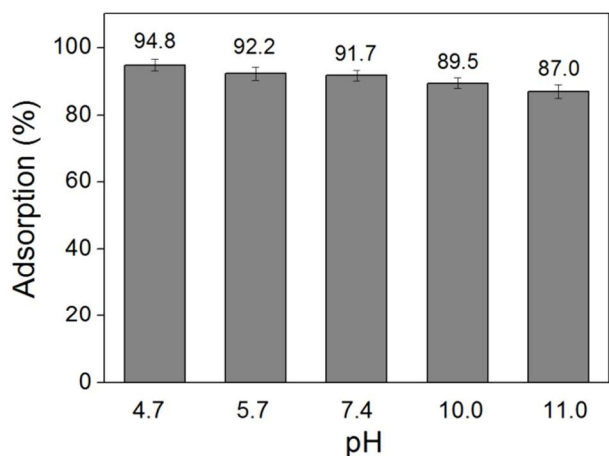
Fig. 3 Effect of pH on polyA$_{25}$ adsorption onto (PEI/HSA)$_5$PEI nanotubes. ((PEI/HSA)$_5$PEI nanotubes dose = 0.1 mg, C_0 = 108 mg/L, t = 1 h).

5 about 30 min. while for concentrations of 58-108mg/L, 50 min was required. For larger concentrations of 163-228 mg/L, a longer time of 300 min was necessary. The effect of initial polyA$_{25}$ concentration on adsorption was also observed. A rise of concentration from 22 mg/L to 228 mg/L caused an increase in 10 the amount of equilibrium adsorption from 42.1 mg/g to 392.0 mg/g, which was ascribed to more availability of polyA$_{25}$ to the active sites on nanotubes at higher concentration.

In order to understand the mechanism of adsorption kinetics, three types of kinetic model, the pseudo-first-order, pseudo-15 second-order and intra-particle diffusion models, were used to analyze the experimental dates above.

The pseudo-first-order and pseudo-second-order kinetics[26,27] are expressed as:

$$\ln(q_e - q_t) = \ln q_e - k_1 t \quad (3)$$

$$\frac{t}{q_t} = \frac{1}{k_2 q_e^2} + \frac{t}{q_e} \quad (4)$$

Where k_1 (1/min) and k_2 (g/(mg min)) are the rate constants of pseudo-first-order and pseudo-second-order equations, respectively.
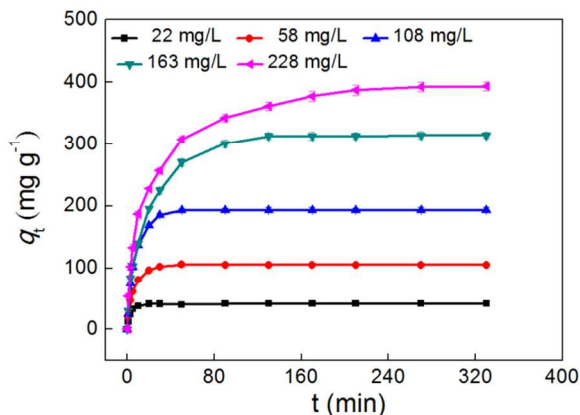
25 **Fig. 4** Effect of adsorption time on polyA$_{25}$ adsorption onto (PEI/HSA)$_5$PEI nanotubes ((PEI/HSA)$_5$PEI nanotubes dose = 0.1 mg, C_0 = 22-228 mg/L, pH = 7.4 ± 0.2).

q_e (mg/g) and q_t (mg/g) are the amount of adsorbed polyA$_{25}$ at equilibrium and t time, respectively .

30 As shown, Fig. 5A and B were the fit of the pseudo-first-order and pseudo-second-order models, respectively. The obtained kinetic parameters were listed in Table 1. It was found the pseudo-second-order equation fitted better than the pseudo-first-order model by comparing the correlation coefficients. The 35 calculated values $q_{e,cal}$ (*i.e.* 42.4, 111.1, 196.5, 325.7, 408.2 mg/g) from the former were close to the experimental values $q_{e,exp}$ (*i.e.* 42.1, 106.1, 195.1, 315.0, 392.0 mg/g), suggesting that the pseudo-second-order kinetics more suitably described the adsorption of polyA$_{25}$.

40
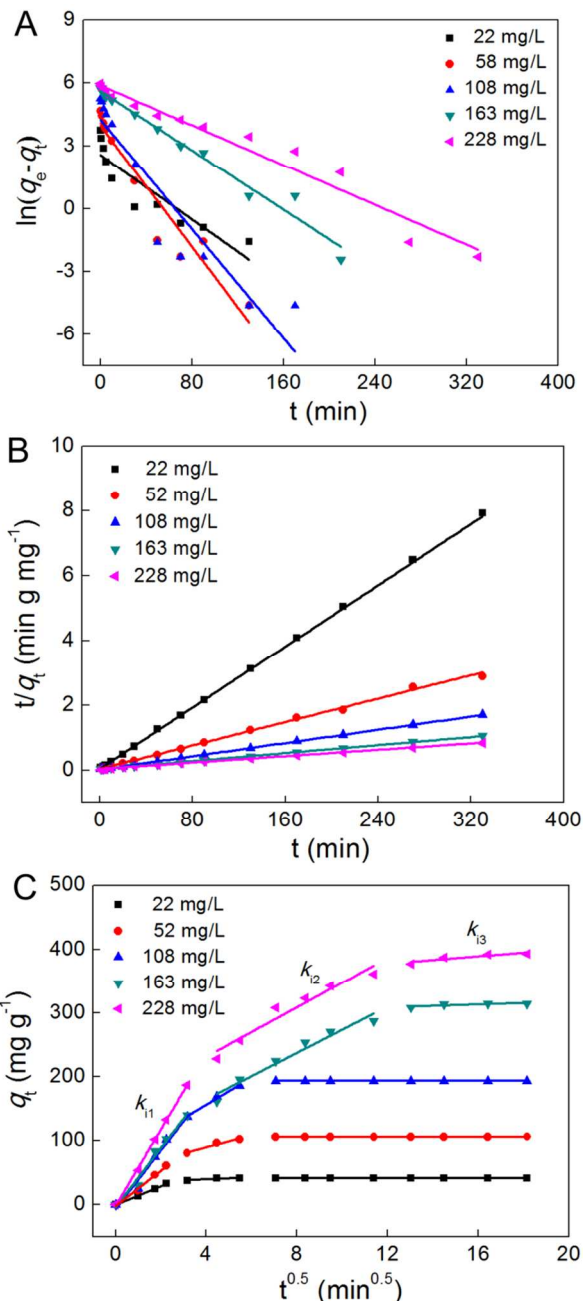
Fig. 5 (A) The pseudo-first-order kinetic model, (B) The pseudo-second-order kinetic model, (C) The intra-particle diffusion model for polyA$_{25}$ adsorption onto (PEI/HSA)$_5$PEI nanotubes.

Table 1 Comparison of pseudo-first-order, pseudo-second-order kinetic and intra-particle diffusion models parameters, calculated values $q_{e,cal}$ and experimental values $q_{e,exp}$ for different initial concentrations of polyA$_{25}$ adsorption onto (PEI/HSA)$_5$PEI nanotubes.

Model	Parameter	C_o (mg/L)				
		22	58	108	163	227
	$q_{e,exp}$ (mg/g)	42.1	106.1	195.1	315.0	392.0
Pseudo-frist-order	k_1 (min^{-1})	0.0384	0.0721	0.0652	0.0354	0.0238
	$q_{e,cal}$ (mg/g)	13.1	52.5	70.8	273.2	361.0
	R^2	0.7967	0.9149	0.8688	0.9746	0.9576
Pseudo-second-order	k_2 (g/(mg min))	0.0147	0.0021	0.0015	0.0003	0.0019
	$q_{e,cal}$ (mg/g)	42.4	111.1	196.5	325.7	408.2
	R^2	0.9999	0.9997	0.9996	0.9993	0.9987
Intra-particle diffusion	k_{i1} (mg/(g min$^{0.5}$))	14.6	26.4	45.7	46.2	59.8
	R^2	0.9958	0.9866	0.9707	0.9753	0.9986
	k_{i2} (mg/(g min$^{0.5}$))	1.44	9.60	21.1	18.2	19.4
	R^2	0.9032	0.9292	0.9754	0.9502	0.9316
	k_{i3} (mg/(g min$^{0.5}$))	0.0204	0.0344	0.0399	1.11	2.89
	R^2	0.9382	0.9795	0.9363	0.9191	0.9503

5

The adsorption process was further analyzed using the intra-particle diffusion model[28] expressed as:

$$q_t = k_i t^{0.5} \qquad (5)$$

Where k_i (mg/(g min$^{0.5}$)) is the rate constant of intra-particle
10 diffusion. The value of k_i can be calculated from the slope of plot q_t versus $t^{0.5}$.
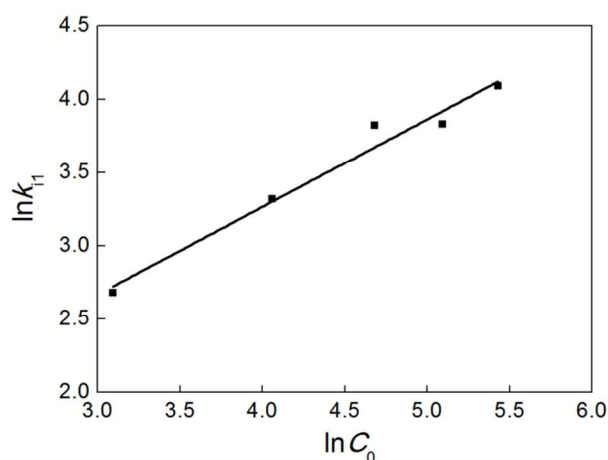
Fig. 6 Plot of $\ln k_{i1}$ against $\ln C_0$ for polyA$_{25}$.

Table 2 Values of rate parameter constants in equation.

Material	Parameter	Parameter Value
polyA$_{25}$	A_n	2.40
	B_n	0.59
	R^2	0.9653

15

Three regions were seen from the plots of q_t versus $t^{0.5}$ at different initial concentrations of 22-228 mg/L, which represented the three consecutive mass transport steps in adsorption (Fig. 5C). The rates of adsorption at corresponding
20 stages expressed as k_{i1}, k_{i2}, k_{i3} could be derived from the slopes of linear portions. The first stage also the fastest (k_{i1}) was attributed to large amounts of polyA$_{25}$ diffusion to the external surface of nanotubes. The second portion (k_{i2}) was the stage of polyA$_{25}$ migrating into the pores. With concentration of polyA$_{25}$
25 decreasing in solution, the intra-particle diffusion gradually slowed down until reached the equilibrium stage (k_{i3}). As listed in Table 1, the rate was $k_{i1} > k_{i2} > k_{i3}$, and the values increased as initial concentration increased, since the intra-particle diffusion model was based on Fick's Law. k_{i3} was larger at higher initial
30 concentration and thus longer equilibrium time was needed, which well interpreted the experimental results of equilibrium time needed.

The correlation of rate parameter k_{i1} and initial concentration[28] was represented as following, and the plot of $\ln k_{i1}$ versus $\ln C_0$ was
35 shown in Fig. 6.

$$k_{i1} = A_n C_o^{B_n} \qquad (6)$$

The values of constant were listed in Table 2.

3.4 Adsorption isotherm

The Langmuir and Freundlich isotherm equations are the typical
40 models to predict the adsorption type of adsorbate on an adsorbent. The Langmuir isotherm equation is based on monolayer adsorption on a homogeneous surface of adsorbent[29] and the linear form is expressed as:

$$\frac{C_e}{q_e} = \frac{1}{bQ^0} + \frac{C_e}{Q^0} \qquad (7)$$
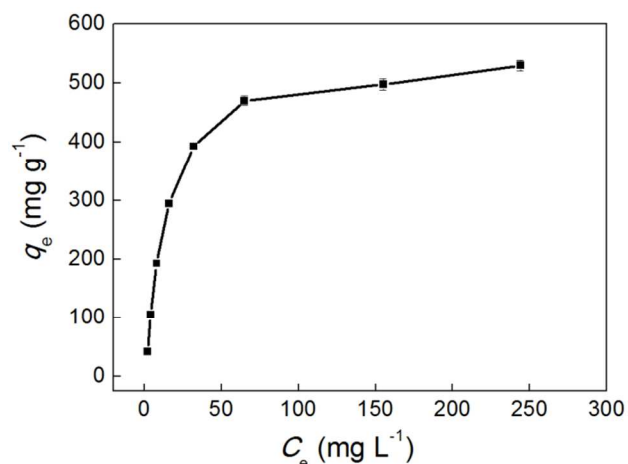
Fig. 7 PolyA$_{25}$ adsorption isotherm of (PEI/HSA)$_5$PEI nanotubes. ((PEI/HSA)$_5$PEI nanotubes dose = 0.1 mg, C_0 = 22-500 mg/L, t = 8 h, pH = 7.4 $\pm$ 0.2).

5

Where C_e (mg/L) is the equilibrium concentration of polyA$_{25}$, q_e (mg/g) is the amount of adsorbed polyA$_{25}$ at equilibrium, b (L/mg) and Q^0 (mg/g) are Langmuir constants related to adsorption energy and adsorption capacity, respectively. The
10 values of Q^0 and b can be calculated from the slope and intercept of plot C_e/q_e versus C_e.

A dimensionless equilibrium parameter (R_L)[29], which is represented as:

$$R_L = \frac{1}{1+bC_0} \qquad (8)$$

15 Where b (L/mg) is Langmuir constant, C_0 (mg/L) is the highest polyA$_{25}$ concentration. The value of R_L means the type of isotherm to be either unfavorable ($R_L > 1$), linear ($R_L = 1$), favorable ($R_L < 1$) or irreversible ($R_L = 0$).

The Freundlich isotherm model is regarded as adsorption on a
20 heterogeneous surface[30] and expressed as:

$$\ln q_e = \ln K_F + \frac{1}{n}\ln C_e \qquad (9)$$

Where K_F (mg/g) and n are the Freundlich constants related to adsorption capacity and adsorption intensity, respectively. The values of 1/n and K_F can be obtained from the slope and intercept
25 of plot $\ln q_e$ versus $\ln C_e$.

Table 3 Isotherm parameters for polyA$_{25}$ adsorption on (PEI/HSA)$_5$PEI nanotubes.

Model	parameter	parameter value
Langmuir	Q^0 (mg/g)	606.0
	b (L/mg)	0.048
	R^2	0.9944
	R_L	0.04
Freundlich	$1/n$	0.48
	K_F (mg/g)	52.9
	R^2	0.8246

30 The isotherm curve of polyA$_{25}$ adsorption on (PEI/HSA)$_5$PEI nanotubes was presented in Fig. 7 and the fitting models by Langmuir and Freundlich isotherm equations were shown in Fig. 8. The derived parameters were summarized in Table 3.

As seen, Langmuir model (R^2 = 0.9944) proved to be more
35 fitted for describing the adsorption process, demonstrating that a monolayer adsorption occurred. The calculated maximum monolayer adsorption capacity (Q^0) was 606.0 mg/g. The low value of b (< 1) implied (PEI/HSA)$_5$PEI nanotubes had a high affinity to polyA$_{25}$. Additionally, polyA$_{25}$ adsorption onto
40 nanotubes was also favorable reasoned from the value of R_L (< 1).

3.5. Comparison adsorption capability with nanoparticles

Compared with spherule allophane nanoparticles (45.0 mg/g)[31] and PEI-modified Fe$_3$O$_4$/Au nanoparticles (90.0 mg/g)[32], the
45 adsorption amount of (PEI/HSA)$_5$PEI nanotubes is 606.0 mg/g. This is the strongest DNA adsorption loader in all previous reports. The excellent absorptivity of (PEI/HSA)$_5$PEI nanotube benefits from its large surface area, unique hollow structure and sufficient DNA binding sites on both outer and inner surfaces. In
50 addition, two open-end terminals make it possible that DNA diffuses into the tube and adsorbs on inner wall.

3.6. DNA Release

The sample of DNA-loaded (PEI/HSA)$_5$PEI nanotubes with adsorbed amount of 195.1 mg/g was used to investigate ionic
55 strength induced release behaviours. As shown in Fig. 9, there
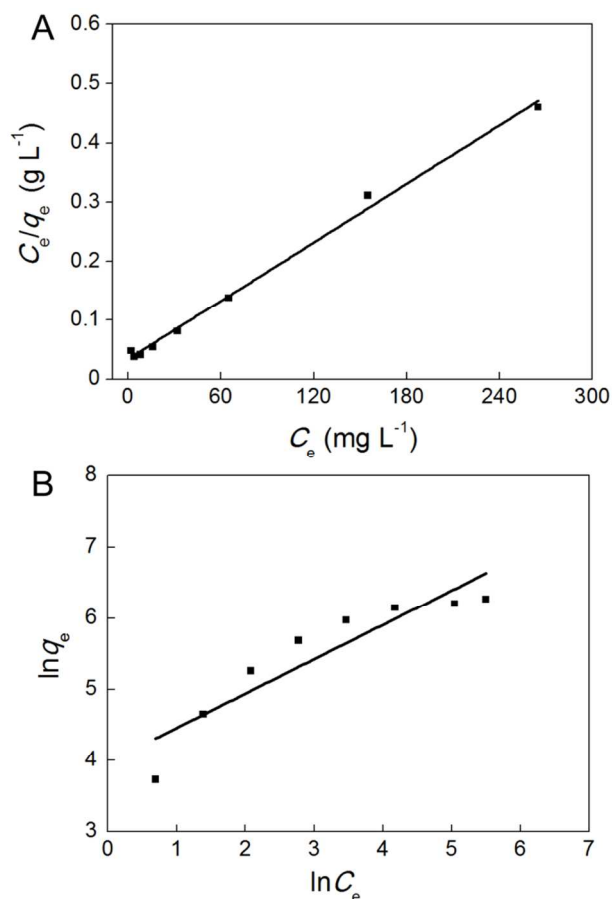
Fig. 8 Fitting by (A) Langmuir model and (B) Freundlich model for polyA$_{25}$ adsorption onto (PEI/HSA)$_5$PEI nanotubes.
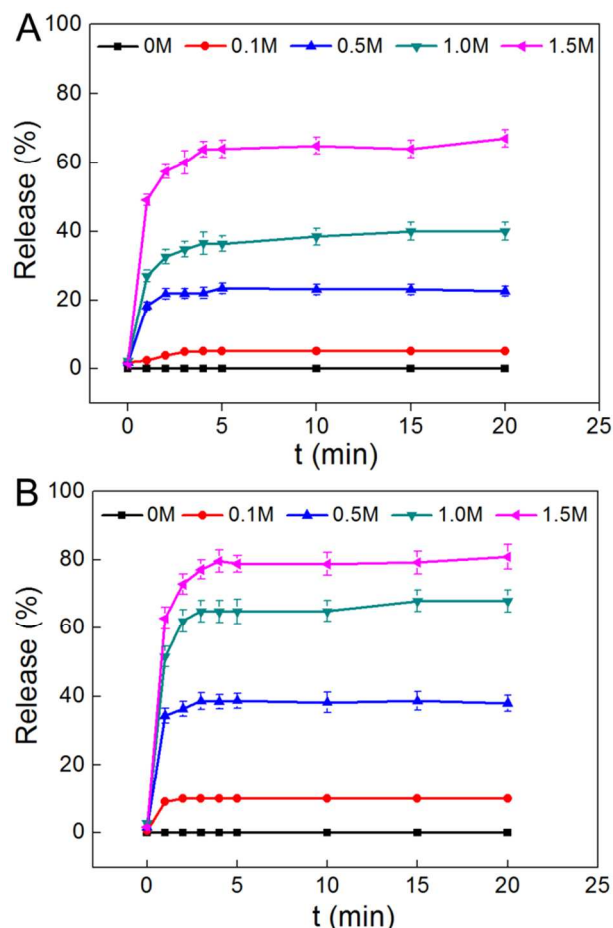
Fig. 9 Kinetics of polyA$_{25}$ release from (PEI/HSA)$_5$PEI nanotubes at (A) pH 7.4 ± 0.2 and (B) pH 5.7 ± 0.2.

was hardly any DNA released in the absence of NaCl. Once NaCl was added, the amount of DNA in solution quickly increased and gave a fast desorption kinetics. For example, by varying NaCl concentration from 0.1 M to 1.5 M, the release ratio increased from 5% to 67.1% at pH 7.4 and from 10% to 78.8% at pH 5.7 in 5 minutes, which might be in that the electrostatic interaction between polyA$_{25}$ and (PEI/HSA)$_5$PEI nanotubes was sensitive in a relatively high ionic strength[33]. At the same ionic strength, the ratio at pH 5.7 was much higher than that of at pH 7.4. This indicated that DNA release from (PEI/HSA)$_5$PEI nanotubes was also pH triggered, providing the necessary conditions for intracellular delivery.

4. Conclusions

In this study, hybrid PEI/HSA nanotubes were successfully prepared with the maximum adsorption capability for polyA$_{25}$ (606.0 mg/g) at pH 7.4 and 25 °C. The adsorption kinetics and isotherm were discussed in detail and demonstrated to fit the pseudo-second-order kinetic, intra-particle diffusion and Langmuir isotherm model. DNA release from DNA/(PEI/HSA)$_5$PEI nanotubes complexes was mainly controlled by the ionic strength and also influenced by pH of solution. In summary, our researches would provide useful information to understand the interaction between DNA and protein nanotubes for design and development of protein nanotubes as gene vectors.

Notes and references

^{a} *Key Laboratory of Synthetic and Natural Functional Molecular Chemistry, College of Chemistry & Materials Science, Northwest University, Xi'an, 710069, P. R. China. Fax: +86-029-81535026.; Tel: +86-029-81535026; E-mail address: guoyl@nwu.edu.cn, kangxf@nwu.edu.cn*

1. E. Huang, F. Zhou and L. Deng, *Langmuir*, 2000, 16, 3272-3280.
2. A. Steel, R. Levicky, T. Herne and M. J. Tarlov, *Biophys. J.*, 2000, 79, 975-981.
3. A. W. Peterson, R. J. Heaton and R. M. Georgiadis, *Nucleic Acids Res.*, 2001, 29, 5163-5168.
4. N. Jirakittiwut, N. Panyain, T. Nuanyai, T. Vilaivan and T. Praneenararat, *RSC Adv.*, 2015, 5, 24110-24114.
5. R. Qi, S. Liu, J. Chen, H. Xiao, L. Yan, Y. Huang and X. Jing, *J. Contr. Rel.*, 2012, 159, 251-260.
6. T. M. Sun, J. Z. Du, L. F. Yan, H. Q. Mao and J. Wang, *Biomaterials*, 2008, 29, 4348-4355.
7. C. R. Martin and P. Kohli, Nat. Rev. *Drug Discov.*, 2003, 2, 29-37.
8. R. Singh, D. Pantarotto, D. McCarthy, O. Chaloin, J. Hoebeke, C. D. Partidos, J.-P. Briand, M. Prato, A. Bianco and K. Kostarelos, *J. Am. Chem. Soc.*, 2005, 127, 4388-4396.
9. C. C. Chen, Y. C. Liu, C. H. Wu, C. C. Yeh, M. T. Su and Y. C. Wu, Adv. Mater., 2005, 17, 404-407.
10. S. J. Son, J. Reichel, B. He, M. Schuchman and S. B. Lee, J. Am. Chem. Soc., 2005, 127, 7316-7317.
11. A. Karlsson, R. Karlsson, M. Karlsson, A.-S. Cans, A. Strömberg, F. Ryttsén and O. Orwar, *Nature*, 2001, 409, 150-152.
12. S. A. Dougherty, D. Zhang and J. Liang, *Langmuir*, 2009, 25, 13232-13237.
13. X. Qu, G. Lu, E. Tsuchida and T. Komatsu, *Chemistry*, 2008, 14, 10303-10308.
14. D. Zhang, S. A. Dougherty and J. Liang, *J. Nanopart. Res.*, 2011, 13, 1563-1571.
15. X. Qu and T. Komatsu, *ACS nano.*, 2009, 4, 563-573.
16. T. Komatsu, X. Qu, H. Ihara, M. Fujihara, H. Azuma and H. Ikeda, *J. Am. Chem. Soc.*, 2011, 133, 3246-3248.
17. S. B. Nimse, K. Song, M. D. Sonawane, D. R. Sayyed and T. Kim, *Sensors*, 2014, 14, 22208-22229.
18. X. Gao, K.-S. Kim and D. Liu, *AAPS J.*, 2007, 9, E92-E104.
19. Y. Liu, D. C. Wu, W. D. Zhang, X. Jiang, C. B. He, T. S. Chung, S. H. Goh and K. W. Leong, *Angew. Chem.*, 2005, 44, 4782-4785.
20. S. Curry, H. Mandelkow, P. Brick and N. Franks, *Nat. Struct. Biol.*, 1998, 5, 827-835.
21. X. M. He and D. C. Carter, *Nature*, 1992, 358, 209-215.
22. J. Kong and S. Yu, *Acta Bioch. Biophy. Sin.*, 2007, 39, 549-559.
23. C. R. Dick and G. E. Ham, *J. Macromol. Sci., Part A*, 1970, 4, 1301-1314.
24. W. Godbey, K. K. Wu and A. G. Mikos, J. Biomed. Mater. Res., 1999, 45, 268-275.
25. M. Wu, R. Kempaiah, P. J. Huang, V. Maheshwari and J. Liu, Langmuir, 2011, 27, 2731-2738.

RSC Advances Accepted Manuscript

26. D. Wang, L. Liu, X. Jiang, J. Yu, X. Chen and X. Chen, *Appl. Surf. Sci.*, 2015, 329, 197-205.

27. H. J. Yan, J. W. Bai, X. Chen, J. Wang, H. S. Zhang, Q. Liu, M. Zhang and L. H. Liu, *RSC. Adv.*, 2013, 3, 23278-23289.

5   28. W. H. Cheung, Y. S. Szeto and G. McKay, *Bioresour. Technol.*, 2007, 98, 2897-2904.

29. B. H. Hameed, A. T. Din and A. L. Ahmad, *J. Hazard. Mater.*, 2007, 141, 819-825.

30. A. A. Ahmad, B. H. Hameed and N. Aziz, *J. Hazard. Mater.*, 2007,
10   141, 70-76.

31. Y. Matsuura, F. Iyoda, S. Arakawa, B. John, M. Okamoto and H. Hayashi, *Mater. Sci. Eng. C Mater. Biol. Appl*., 2013, 33, 5079-5083.

32. H. Sun, X. Zhu, L. Zhang, Y. Zhang and D. Wang, *Mater. Sci. Eng., C*, 2010, 30, 311-315.

15 33. G. S. Irmukhametova, B. J. Fraser, J. L. Keddie, G. A. Mun and V. V. Khutoryanskiy, *Langmuir*, 2012, 28, 299-306.

RSC Advances Accepted Manuscript